Oct 26th, 12:00 AM

Finite Element Modeling of Cold-formed Steel Beams Validation and Application

Cheng Yu

Benjamin W. Schafer

Eighteenth International Specialty Conference on Cold-Formed Steel Structures
Orlando, Florida, U.S.A, October 26 & 27, 2006

Finite Element Modeling of Cold-Formed Steel Beams: Validation and Application

Cheng Yu[1], Benjamin W. Schafer[2]

ABSTRACT

A nonlinear finite element (FE) model is developed herein to simulate two series of flexural tests, previously conducted by the authors, on industry standard C- and Z-section cold-formed steel members. The first test series focuses on local bucking failures and the second on distortional buckling failures. The objectives of this paper are to (i) validate the developed FE model, (ii) apply this model in a parametric study outside the bounds of the original tests with a particular focus on yield stress, and (iii) study the influence of moment gradient on distortional buckling failures. The predicted ultimate strengths from the developed FE model have good agreement with the test data. Extension of the tested sections to cover yield stresses from 33.0 to 73.4 ksi (228 to 506 MPa) indicates that the Direct Strength Method is applicable over this full range of yield stresses. The FE model was also applied to analyze the effect of moment gradient on distortional buckling. It is proposed and verified that the moment gradient effect on distortional buckling failures can be conservatively accounted for in the Direct Strength Method by using an elastic buckling moment that properly reflects the increased elastic distortional buckling moment due to the presence of moment gradient. An empirical equation, appropriate for use in design, to predict the increase in the elastic distortional buckling moment due to moment gradient, is provided.

[1] Assistant Professor, University of North Texas (cyu@unt.edu)
[2] Assistant Professor, Johns Hopkins University (schafer@jhu.edu)

INTRODUCTION

Laterally braced cold-formed steel beams generally suffer from one of two potential instabilities: local or distortional buckling. An extensive series of tests was performed on industry standard cold-formed steel C and Z-beams to study local buckling (Yu and Schafer 2002, 2003) and distortional buckling (Yu and Schafer 2004, 2006) failures. Each test consisted of a pair of 18 ft (5.5 m) long C or Z-sections which were oriented in an opposed fashion and loaded at the 1/3 points along the length.

In the "local buckling tests" a corrugated panel was through-fastened to the compression flange, as shown in Figure 1. The panel stabilizes the compression flange, and specific fastener details were developed to avoid distortional buckling, but allow local buckling. In the "distortional buckling tests" nominally identical specimens were employed, but the corrugated panel attached to the compression flange was removed in the constant moment region, so that distortional buckling could occur, as shown in Figure 2.

A detailed nonlinear finite element model of these two series of tests was first reported in Yu and Schafer (2004). The validation work provided in that paper is briefly reviewed here, followed by two applications: (1) extension of the experimentally studied sections primarily to examine the importance of yield stress variation; and (2) examination of the influence of moment gradient on distortional buckling of cold-formed steel beams.

Figure 1 Local buckling test

Figure 2 Distortional buckling test

FINITE ELEMENT MODELING

Modeling Details and Loading/Boundary Conditions

An overall view of the developed FE model is provided in Figure 3a. The cold-formed steel beams, panel, and hot-rolled tubes (which stiffen the section at the load and support points) are modeled using 4-node, quadrilateral, shell elements (S4R in ABAQUS). The ends of the beams are simply supported at the bottom

flanges under the two end tubes. Connection details and constraints between the beams, the hot-rolled steel tube, the load beam, and the panel are illustrated in Figures 3b and 3c. Link constraints are used to tie the tension flanges of the beams together at the location of the attached angles (see Figure 1 or 2).

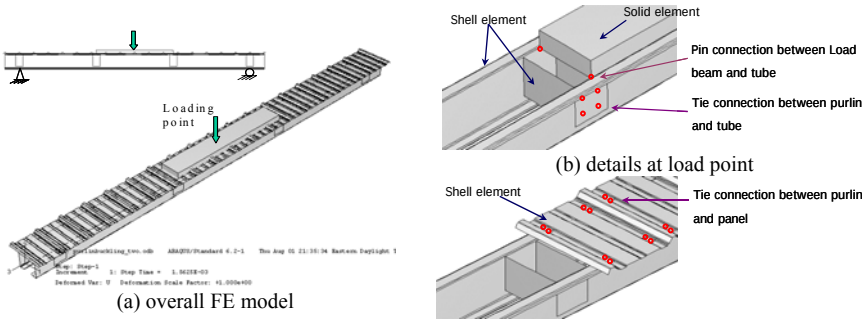

(a) overall FE model

(b) details at load point

(c) details at panel to section

Figure 3 Finite element modeling of beams in local buckling tests.

Geometric Imperfections

Geometric imperfections of the tested beams were not measured. Therefore, the imperfections were based on Schafer and Peköz (1998). We conservatively assumed that the type 1 imperfection may be applied to the local buckling mode and the type 2 imperfection applied to the distortional buckling mode. For each test, two FE simulations were performed. One simulation used a larger initial geometric imperfection with a 75% CDF magnitude (d_1/t = 0.66 for local buckling; d_2/t = 1.55 for distortional buckling), the other used a smaller magnitude with 25% CDF magnitude (d_1/t = 0.14 for local buckling; d_2/t = 0.64 for distortional buckling), thus covering the middle 50% of anticipated imperfection magnitudes. The final imperfection shape is a scaled superposition of the local and distortional buckling modes.

Material Modeling

Material nonlinearity in the cold-formed steel beams was modeled with von Mises yield criteria and isotropic hardening. Measured stress-strain relations taken from tensile coupons from the beams were employed. All other components were modeled as elastic, with E = 29500 ksi (203 GPa) and ν = 0.3, except for the hot-rolled steel tubes and the loading beam which used an artificially elevated modulus (10E) so that they would effectively act as rigid bodies. Residual stresses were ignored.

Comparison with Experimental Results

As demonstrated in Figure 4, the developed FE model provides a good prediction of the deformed shapes. The local buckling test is characterized by

short and repeated buckling waves. The distortional buckling test failed with the compression flange rotating, and with a longer buckling wavelength than that in the local mode.

(a) 11.5Z092-1E2W local buckling test

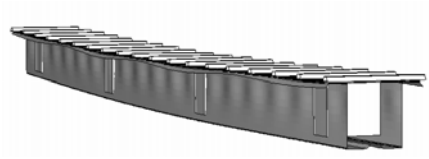

(b) Simulation of local buckling test

(c) 11.5Z092-3E4W distortional buckling test

(d) Simulation of distortional buckling test

Figure 4 General comparison of test and FE models

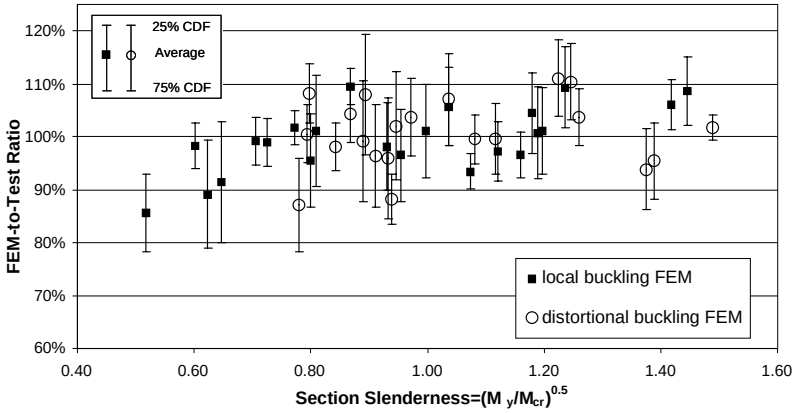

Figure 5 Accuracy and sensitivity of FE predictions for tested beams

The results of the finite element analyses are illustrated in Figure 5 and summarized in Table 1. The mean response of the FEM simulations has good agreement with the tested strength. The pair of simulations also provide a measure of imperfection sensitivity: the middle 50% of expected imperfection magnitudes result in a range of bending capacity equal to 13% for local buckling and 15% for distortional buckling.

Table 1 Summary of finite element analysis results for local buckling tests

	Test label	$P_{25\%\sigma}/P_{test}$	$P_{75\%\sigma}/P_{test}$	P_{mean}/P_{test}
Local buckling tests	mean	106%	93%	100%
	standard deviation	6%	7%	6%
Distortional buckling tests	mean	108%	93%	101%
	standard deviation*	7%	7%	6%

Note: P_{test}: Peak tested actuator load; P_{mean}: Average value of $P_{25\%\sigma}$: and $P_{75\%\sigma}$;
$P_{25\%\sigma}$: Peak load of simulation with 25% CDF of maximum imperfection;
$P_{75\%\sigma}$: Peak load of simulation with 75% CDF of maximum imperfection.

Some limitations exist with the developed FE model. For example, a trend with respect to slenderness is observable (Figure 5). This is likely due to our imperfection choice, which is a function of thickness. Further, the post-collapse mechanism is not always well approximated. Lack of agreement in the large deflection post-collapse range could be a function of the solution scheme (i.e., use of artificial damping instead of Riks) or more basic modeling assumptions, such as ignoring plasticity in the panels and the contact between components of the beam. Further discussion of the issues raised above and complete details of the modeling results may be found in Yu (2005). In total, it is concluded that the ultimate strength for both local buckling and distortional buckling of cold-formed steel beams is well simulated by this finite element model, and thus the model is considered to be validated and used for further study in this paper.

APPLICATION I: EXTENDED FINITE ELEMENT ANALYSIS AND APPLICATION OF THE DIRECT STRENGTH METHOD

Given the successful verification of the developed finite element model, extension to a greater variety of cold-formed steel sections and material properties (not examined experimentally) is possible. Of particular interest was a further examination of yield stress on the behavior. This was primarily driven by the fact that experimentally measured yield stress for the Z-sections showed little variation, but for the C-sections covered an extensive range. A subset of the tested sections, covering yield stresses from 33.0 to 73.4 ksi (228 to 506 MPa), and with stress-strain curves based on experimentally measured coupons, was employed in this extended finite element analysis study. The FE results from these models are compared with Direct Strength Method (NAS 2004, Schafer and Peköz 1998) predictions in this section.

Models of both the local buckling test and distortional buckling test (no panel attached to the compression flange in the pure bending region) were completed. A subset of the tested geometries was selected, as given in Table 2. The method of generating geometric imperfections described in the previous section was again employed. The maximum imperfection magnitude was selected to

correspond to a 50% probability of exceedance (50% CDF: $d_1/t = 0.34$ for local buckling mode; $d_2/t = 0.94$ for distortional buckling mode).

Table 2 Geometry and yield stress of analyzed sections

Specimen	h (in.)	b_c (in.)	d_c (in.)	θ_c (deg)	b_t (in.)	d_t (in.)	θ_t (deg)	r_{hc} (in.)	r_{dc} (in.)	r_{ht} (in.)	r_{dt} (in.)	t (in.)
8Z2.25x050	8.0	2.3	0.9	50	2.3	0.9	50	0.24	0.24	0.24	0.24	0.0500
8Z2.25x100	8.0	2.3	0.9	50	2.3	0.9	50	0.24	0.24	0.24	0.24	0.0500
8.5Z2.5x70	8.5	2.5	0.9	50	2.5	0.9	50	0.25	0.25	0.25	0.25	0.0700
8.5Z092	8.4	2.6	0.9	51.8	2.4	1.0	50.4	0.28	0.28	0.31	0.31	0.0900
8.5Z120	8.5	2.6	1.0	47.8	2.5	1.0	48.9	0.36	0.36	0.34	0.34	0.1176
8.5Z082	8.46	2.50	0.95	49.0	2.36	0.97	50.3	0.28	0.28	0.30	0.30	0.0806
11.5Z3.5x80	11.5	3.5	0.9	50	3.5	0.9	50	0.30	0.30	0.30	0.30	0.0800
8C068	7.9	1.9	0.7	80	2.0	0.6	77.8	0.16	0.16	0.16	0.16	0.0700
8C097	8.04	2.09	0.58	85.1	2.07	0.53	86.3	0.28	0.28	0.29	0.28	0.0980
12C068	12.00	2.00	0.60	85.0	2.00	0.60	85.0	0.26	0.27	0.26	0.26	0.0680

yield stress, f_y = 33.0, 44.0, 56.1, 62.2, and 73.4 ksi

The Performance of the Direct Strength Method

Figure 6a shows a comparison of the local buckling strength of cold-formed steel beams calculated by the Direct Strength Method (DSM) with data from both the tests and the extended FEM simulations. A similar comparison for distortional buckling is provided in Figure 6b. Table 3 summarizes the comparison of DSM predictions with both the tested and extended FEM model bending capacities. In general, DSM provides reliable and conservative predictions for the bending strength of cold-formed steel beams. The local buckling strength predictions are more scattered than those of distortional buckling, and significant inelastic reserve is ignored.

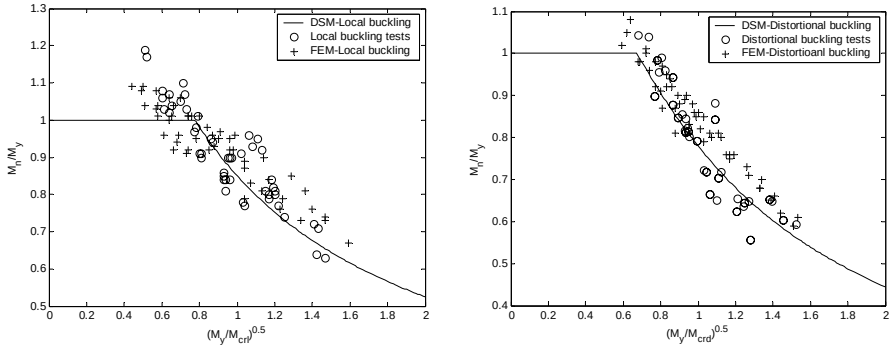

(a) local buckling (b) distortional buckling

Figure 6 Comparison of DSM to tests and extended FE results

Table 3 Summary of DSM predictions vs. test and FEM results

		Local buckling		Distortional buckling	
		M_n/M_{DSM}	Number	M_n/M_{DSM}	Number
Tests	μ	1.03	23	1.01	18
	σ	0.06	23	0.07	18
FEM	μ	1.02	50	1.04	50
	σ	0.07	50	0.07	50
Overall	μ	1.03	73	1.03	68
	σ	0.07	73	0.07	68

Note: μ – average; σ – standard deviation;
M_n – bending capacity of beams (test or ABAQUS);
M_{DSM} – predictions of Direct Strength Method;
Number – the number of analyzed sections.

APPLICATION II: MOMENT GRADIENT EFFECT ON DISTORTIONAL BUCKLING

In practical situations beams are subjected to a variety of moment gradients. In design, moment gradient is considered in the calculation of lateral-torsional buckling (i.e., C_b) but ignored in local and distortional buckling. In the local mode the buckling half-wavelength is short and the moment gradient has only a minor influence (particularly for stiffened elements, see Yu and Schafer 2004b, 2006b). However, in the distortional mode the buckling half-wavelength seems long enough that typical moment gradients could have influence. The question is of some practical significance, because one common case for concern in distortional buckling is the negative bending region of a continuous beam (Figure 7). Significant moment gradients exist in this region, and in practice little restraint may be placed on the bottom flanges.

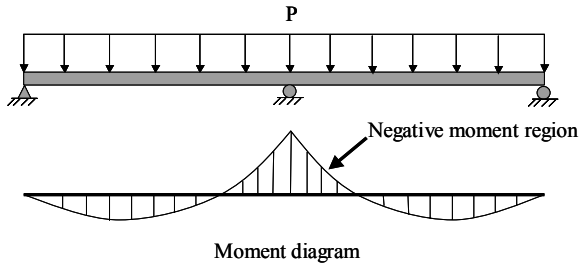

Figure 7 A continuous beam under uniform distributed loads

In this section, the moment gradient effect on both elastic buckling and ultimate strength of cold-formed steel beams failing in distortional buckling is analyzed by finite element models.

Elastic Distortional Buckling under Moment Gradient

The first step is to examine the moment gradient effect on the elastic distortional buckling moment (M_d) of cold-formed steel beams. For example, see the work of Bebiano et al. (2006). Here, an FE model (in ABAQUS) is utilized to determine M_d under a linear moment gradient, r (where $r = M_1/M_2$, M_1 and M_2 are the end moments, $|M_2| > |M_1|$). The developed FE model is shown in Figure 8a, along with the resulting elastic distortional buckling modes under varying moment gradients: Figures 8b–d.

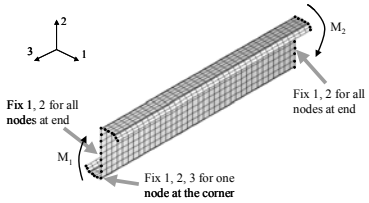

(a) FE model for moment gradient, $L=3L_{crd}$

(b) constant moment (r = 1)

(c) linear moment gradient (r = 0)

(d) double curvature (r = -1)

Figure 8 FE model and distortional buckling of Z-section with moment gradient

Twelve typical cold-formed steel C and Z-sections are chosen for detailed elastic distortional buckling FE analysis, see Table 5. For the selected sections the influence of linear moment gradient (r) on the elastic distortional bucking moment (M_d) of a beam of fixed length ($L = 3L_{crd}$) is shown in Figure 9; where, L_{crd} is the half-wavelength and M_{crd} is the elastic buckling moment for distortional buckling under constant moment (r = 1). The elastic distortional buckling moment is increased when a moment gradient is applied. For example, when r = -1 (double curvature) a 30% to 50% increase is observed.

Figure 9 shows that moment gradient has an influence on elastic distortional buckling, but if the same moment gradient occurs over a longer length of the beam this influence will dissipate. For a triangular bending moment diagram (r = 0) this dissipation is illustrated in Figure 10. Theoretically, as $L \rightarrow \infty$, the buckling moment will converge to the case with no moment gradient (i.e., M_{crd}), but the FE analysis indicates convergence to these limiting values is slow. For beams with a length of $10L_{crd}$, a minimum 10% increase in M_d above M_{crd} is still observed. A lower bound of the moment gradient effect for r = 0 is:

$$M_d / M_{crd} = 1.0 \le 1.0 + 0.4\left(\frac{L_{crd}}{L}\right)^{0.7} \le 1.3 \quad (1)$$

Table 4 Geometry of selected sections for study

type	label	h (in.)	b_c (in.)	d_c (in.)	θ_c (deg)	b_t (in.)	d_t (in.)	θ_t (deg)	r_{hc} (in.)	r_{dc} (in.)	r_{ht} (in.)	r_{dt} (in.)	t (in.)
Z	8Z50	8.00	2.25	0.93	50.0	2.25	0.93	50.0	0.24	0.24	0.24	0.24	0.0500
	8Z100	8.00	2.25	0.93	50.0	2.25	0.93	50.0	0.24	0.24	0.24	0.24	0.1000
	11.5Z100	11.50	3.50	0.90	50.0	3.50	0.90	50.0	0.30	0.30	0.30	0.30	0.1000
	8.5Z070	8.50	2.50	0.90	50.0	2.50	0.90	50.0	0.25	0.25	0.25	0.25	0.0700
	8.5Z082	8.46	2.50	0.95	49.0	2.36	0.97	50.3	0.28	0.28	0.30	0.30	0.0806
	8.5Z120	8.47	2.59	0.96	47.8	2.46	1.00	48.9	0.36	0.36	0.34	0.34	0.1176
	8.5Z092	8.43	2.61	0.92	51.8	2.40	0.95	50.4	0.28	0.28	0.31	0.31	0.0900
	11.5Z080	11.50	3.50	0.90	50.0	3.50	0.90	50.0	0.30	0.30	0.30	0.30	0.0800
C	8C097	8.04	2.09	0.58	85.1	2.07	0.53	86.3	0.28	0.28	0.29	0.28	0.0980
	8C054	8.00	2.05	0.59	89.4	2.04	0.56	83.3	0.22	0.23	0.23	0.24	0.0520
	10C068	10.10	2.07	0.53	80.7	2.08	0.52	81.9	0.24	0.23	0.23	0.22	0.0634
	3.62C054	3.73	1.88	0.41	87.0	1.87	0.43	89.0	0.26	0.24	0.27	0.27	0.0555

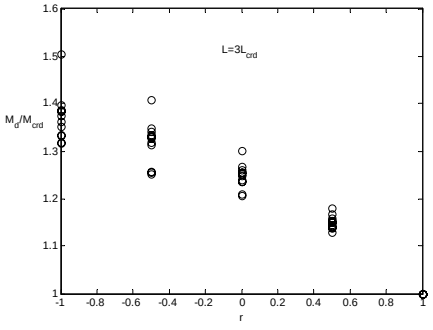

Figure 9 Moment gradient ($r = M_1/M_2$) influence on elastic distortional buckling

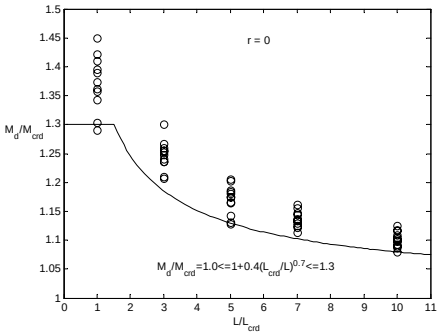

Figure 10 Section length ratio influence on elastic distortional buckling

The moment gradient factor r, and section length ratio L_{crd}/L, are two essential parameters for representing the moment gradient influence. An "equivalent moment concept" is proposed here as an approximate method to simplify the possible loading configurations (different r and L_{crd}/L) to a single case, as shown in Figures 11a and b. The equivalent moment concept presumes that the elastic distortional buckling moment of a beam with length L and moment gradient $r = M_1/M_2$ is equal to the elastic distortional buckling moment of the same section with length L_e under moment gradient r = 0.

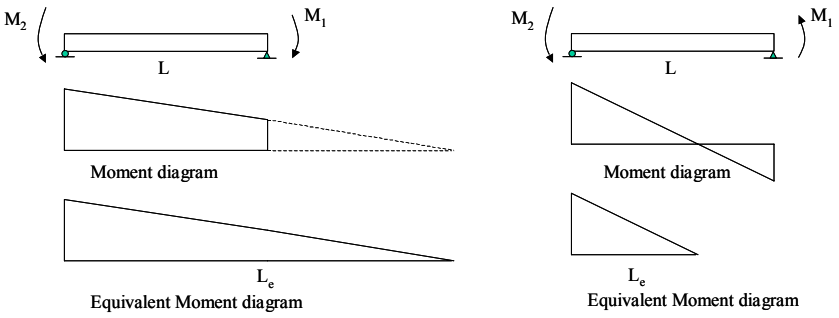

(a) single curvature (b) double curvature

Figure 11 Equivalent moment concept for elastic distortional buckling prediction

A series of finite element analyses were performed to examine the equivalent moment concept. Three cases were studied: (1) $L = 3L_{crd}$, $r = 0$; (2) $L = 1.5L_{crd}$, $r = 0.5$; (3) $L = 4.5L_{crd}$, $r = -0.5$. The equivalent moment concept presumes that these three cases have the same elastic distortional buckling moment (i.e., M_d based on $L_e=3L_{crd}$, $r=0$). The FE results are summarized in Table 5, and it is shown that the distortional buckling moment of these three cases, for each section, are indeed quite close; the difference is below 3% on average. The equivalent moment concept is a simplification with validity, at least for the studied sections.

Using the equivalent moment concept, all moment gradient effects can be projected to the same case in which a moment gradient $r = 0$ is applied to the beam with the equivalent length L_e, and Eq. 1 can be generalized to:

$$M_d/M_{crd} = 1.0 \le 1 + 0.4(L_{crd}/L)^{0.7}(1 - M_1/M_2)^{0.7} \le 1.3 \qquad (2)$$

where M_2 and M_1 are the end moments on a beam of length L;
$|M_2| > |M_1|$, single curvature is positive;
L_{crd} is the half wavelength of distortional buckling under constant moment ($M_1=M_2$);
M_{crd} is the distortional buckling moment under constant moment ($M_1=M_2$);
M_d is the distortional buckling moment under a moment gradient $r=M_1/M_2$ ($M_1 \neq M_2$).

Table 5 Finite element results for Equivalent Moment Concept

Section label	M_{crd-1} (kip-in.) ($r = 0$, $L = 3L_{crd}$)	M_{crd-2}/M_{crd-1} ($r = 0.5$, $L = 1.5L_{crd}$)	M_{crd-3}/M_{crd-1} ($r = -0.5$, $L = 4.5L_{crd}$)
8Z50	73.33	1.02	0.99
8Z100	323.13	1.03	0.99
11.5Z100	342.36	1.03	1.00
8.5Z070	150.34	1.04	1.00
8.5Z082	205.23	1.03	0.99
8.5Z120	451.59	1.03	1.00
8.5Z092	257.51	1.03	0.99
11.5Z080	213.73	1.02	1.00
8C097	317.85	1.04	0.94
8C054	80.78	1.03	0.99
10C068	115.94	0.97	0.95
3.62C054	45.74	1.03	1.00
	Average	1.03	0.99

Ultimate Distortional Buckling Strength under Moment Gradient

In this section, the previously validated nonlinear finite element model is extended to investigate ultimate strength of cold-formed steel beams failing in distortional buckling under a moment gradient. Two nonlinear finite element models were used. The first model, Figure 12, modifies the original test setup to a single load P applied at the first 1/3 point, thus the unrestrained part of beam is subjected to a moment gradient r = 0.5. The second model, Figure 13, replaces the constant moment region with a single mid-span applied load and braces the compression flange with corrugated panel on one side only, thus the beam is subjected to a moment gradient r = 0. A local and distortional buckling combined mode shape is selected for the initial geometric imperfection, and the magnitude corresponds to the 50% CDF. Yield stresses of 33.0, 44.0, 56.1, 62.2, and 73.4 ksi (228, 303, 387, 429, and 506 MPa) based on tensile coupons taken from earlier tested specimens are employed.

Figure 12 shows the deformed shape of beam 11.5Z080 subjected to a moment gradient, r = 0.5, analyzed by the first finite element model, the material yield stress is 62.2 ksi (429 MPa). A distortional buckling wave is observed close to the load point where maximum bending moment exists. The finite element analysis shows the bending capacity of this beam is increased 15% when the moment gradient r = 0.5 is applied.

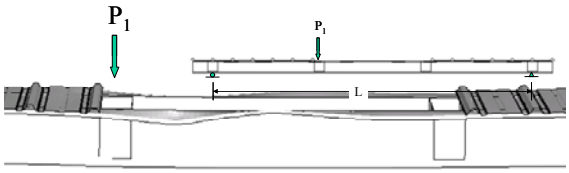

Figure 12 Deformed shape of 11.5Z080 beam subjected to a moment gradient r = 0.5

Figure 13 illustrates the deformed shape of beam 8.5Z070 subjected to a moment gradient r = 0, analyzed by the second finite element model. The distortional buckling half-wave forms next to the load point and the finite element analysis indicates that the strength of the beam is increased 22.5% compared with the same beam under constant moment.

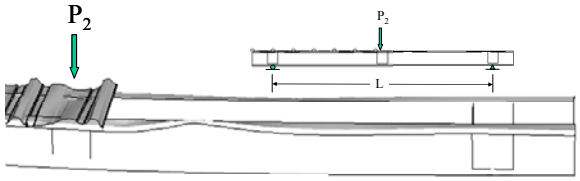

Figure 13 Deformed shape of 8.5Z070 beam subjected to a moment gradient r = 0

The geometry of the C- and Z-sections analyzed by the two FE models is given in Table 6. The numerical results are summarized in Table 7, where it is shown that when compared to simulations of the distortional buckling tests under constant moment, the bending strength in the distortional buckling mode increases by an average of 15% (see $M_{FEd\text{-}MG}/M_{FEd}$ in Table 7) due to the presence of the moment gradient.

Table 6 Geometry of analyzed C and Z-sections

Specimen	h (in.)	b_c (in.)	d_c (in.)	θ_c (deg)	b_t (in.)	d_t (in.)	θ_t (deg)	r_{hc} (in.)	r_{dc} (in.)	r_{ht} (in.)	r_{dt} (in.)	t (in.)
8.5Z082	8.46	2.50	0.95	49.0	2.36	0.97	50.3	0.28	0.28	0.30	0.30	0.0806
8.5Z120	8.47	2.59	0.96	47.8	2.46	1.00	48.9	0.36	0.36	0.34	0.34	0.1176
11.5Z080	11.50	3.50	0.90	50.0	3.50	0.90	50.0	0.30	0.30	0.30	0.30	0.0800
8C097	8.04	2.09	0.58	85.1	2.07	0.53	86.3	0.28	0.28	0.29	0.28	0.0980
8.5Z070	8.50	2.50	0.90	50.0	2.50	0.90	50.0	0.25	0.25	0.25	0.25	0.0700
8Z100	8.00	2.25	0.93	50.0	2.25	0.93	50.0	0.24	0.24	0.24	0.24	0.1000
11.5Z100	11.50	3.50	0.90	50.0	3.50	0.90	50.0	0.30	0.30	0.30	0.30	0.1000
8Z050	8.00	2.25	0.93	50.0	2.25	0.93	50.0	0.24	0.24	0.24	0.24	0.0500

Table 7 Comparisons of DSM predictions with FE results

		M_{FEd-MG}/M_{FEd}	M^*_{DSd-MG}/M_{DSd}	M_{FEd-MG}/M_{DSd-MG}	M_{FEd-MG}/M^*_{DSd-MG}
FE model with r = 0.5	μ	1.13	1.06	1.15	1.14
	σ	0.02	0.03	0.05	0.05
FE model with r = 0	μ	1.25	1.07	1.22	1.20
	σ	0.04	0.02	0.04	0.04
Overall	μ	1.15	1.06	1.16	1.15
	σ	0.05	0.03	0.06	0.05

Note: μ - average; σ - standard deviation

M_{FEd-MG} FE prediction of ultimate moment in distortional buckling with moment gradient

M_{FEd} FE prediction of ultimate moment in distortional buckling no moment gradient

M^*_{DSd-MG} Direct Strength prediction of nominal moment in distortional buckling, with M_{crd} determined by FE elastic buckling including moment gradient influence

M_{DSd-MG} Direct Strength prediction of nominal moment in distortional buckling, with M_{crd} determined from Eq. 2 and includes moment gradient influence

M_{DSd} Direct Strength prediction of nominal moment in dist. buckling no moment gradient

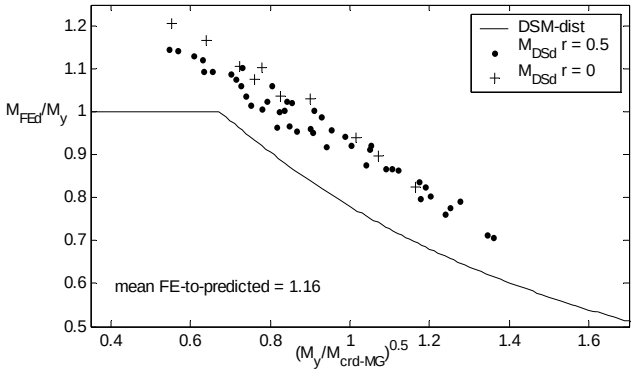

Figure 14 Comparison of the Direct Strength Method distortional buckling prediction with finite element modeling ($M_{crd-MG} = M_d$ of Eq. 2)

It is proposed that the influence of the moment gradient on the strength may be approximated in the Direct Strength Method by allowing the elastic buckling moment M_{crd} in the Direct Strength Method equations to include the influence of moment gradient; i.e., let M_d of the previous section be used in place of M_{crd}. The consequence of this choice is shown in Figure 14, where M_d of Eq. 2 has been used in place of M_{crd} – the result is a conservative approximation to the strength increase observed due to the moment gradient. If the exact M_d is used instead of Eq. 2, the resulting strength prediction (M^*_{Dsd-MG} of Table 7) is slightly improved. Comparison of the accuracy of the Direct Strength equations for distortional bucking failures without moment gradient, Figure 6b, to that of Figure 14 indicates that while the proposed approach is simple it remains a bit

on the conservative side. Indicating that post-buckling and collapse under the moment gradient may be slightly different than in constant moment, an issue that deserves further study.

CONCLUSIONS

A nonlinear FE model was developed (in ABAQUS) and verified against previously conducted flexural tests on cold-formed steel C- and Z-section beams. The FE analysis was extended to cold-formed steel beams not included in the tests; in particular, yield stress was varied from 33.0 to 73.4 ksi (228 to 506 MPa). The results indicate that the Direct Strength Method yields reasonable strength predictions for both local and distortional bucking failures of beams covering a wide range of industry standard C- and Z-sections and yield stresses. The FE model was also utilized to study the distortional buckling and post-buckling behavior of cold-formed steel beams under moment gradients. Moment gradients were achieved by applying uneven loads at the two 1/3 points of the beams as originally tested. The FE results show that overly conservative predictions will be made if the moment gradient effect is ignored. It is also shown that with the appropriate elastic buckling moments, the Direct Strength Method is a conservative predictor of the increased strength due to moment gradient in distortional buckling. The elastic distortional buckling moment under a moment gradient can be determined by finite element analysis, or by the empirical equation proposed here, Eq. 2.

REFERENCES

ABAQUS (2001). "ABAQUS Version 6.2", ABAQUS, Inc, Pawtucket, RI. (www.abaqus.com)

Bebiano, R., Silvestre, N., Camotim, D. (2006). "On the influence of stress gradients on the local-plate, distortional and global buckling behavior of thin-walled steel members", *Proc. of Annual Tech. Session and Meeting*, Structural Stability Research Council, Feb., 2006, San Antonio, TX. pp. 301-327.

NAS (2004). "North American Specification for the Design of Cold-Formed Steel Structural Members: Appendix 1, Design of Cold-Formed Steel Structural Members Using the Direct Strength Method", American Iron and Steel Institute, Washington, D.C.

Schafer, B.W., Peköz, T. (1998). "Computational Modeling of Cold-Formed Steel: Characterizing Geometric Imperfections and Residual Stresses", Elsevier, *J. of Constructional Steel Research*, 47 (3) 193-210.

Schafer, B.W., Peköz, T. (1998b). "Direct strength prediction of cold-formed steel members using numerical elastic buckling solutions", *Proc. of the Fourteenth Int'l Specialty Conf on Cold-Formed Steel Structures*, St. Louis, MO. pp. 69-76.

Yu, C. (2005). "Distortional buckling of cold-formed steel members in bending", *PhD Thesis*, Johns Hopkins University, Baltimore, MD.

Yu, C., Schafer, B.W. (2002). "Local buckling tests on cold-formed steel beams", *Proc. of the Sixteenth Int'l Specialty Conf on Cold-Formed Steel Structures*, Orlando, FL. pp 127-144.

Yu, C., Schafer, B.W. (2003). "Local buckling tests on cold-formed steel beams", *J. of Structural Engineering*, ASCE. 129 (12) 1596-1606.

Yu, C., Schafer, B.W. (2004). "Distortional buckling tests on cold-formed steel Beams", *Proc. of the Seventeenth Int'l Specialty Conference on Cold-Formed Steel Structures*, Orlando, FL. pp 19-46.

Yu, C., Schafer, B.W. (2004b). "Stress gradient effect on the buckling of thin plates", *Proc. of the Seventeenth Int'l Specialty Conference on Cold-Formed Steel Structures*, Orlando, FL. pp 47-70.

Yu, C., Schafer, B.W. (2006). "Distortional buckling tests on cold-formed steel beams", ASCE, *J. of Structural Engineering.* (In Press April 2006)

Yu, C., Schafer, B.W. (2006b). "Stability of thin plates under longitudinal stress gradients", *Proc. of Annual Technical Session and Meeting*, Structural Stability Research Council, Feb. 2006, San Antonio, TX. pp 405-424.